Energy Reports 6 (2020) 92–101

Contents lists available at ScienceDirect

Energy Reports

journal homepage: www.elsevier.com/locate/egyr

Research paper

Preparation and physico-chemical investigation of anatase TiO_2 nanotubes for a stable anode of lithium-ion battery

O. Fasakin [a,b], Kabir O. Oyedotun [b], Mesfin Kebede [c], Mark Rohwer [c], Lukas Le Roux [c], Mkhulu Mathe [c], M.A. Eleruja [a], E.O.B. Ajayi [a], Ncholu Manyala [b,*]

[a] Department of Physics and Engineering Physics, Obafemi Awolowo University, Ile-Ife, Osun State, 220005, Nigeria
[b] Department of Physics, Institute of Applied Materials, SARChI Chair in Carbon Technology and Materials, University of Pretoria, Pretoria, South Africa
[c] Energy Materials, Materials Science and Manufacturing, Council for Scientific and Industrial Research (CSIR), Pretoria 0001, South Africa

ARTICLE INFO

Article history:
Received 12 October 2019
Received in revised form 13 February 2020
Accepted 14 February 2020
Available online 20 February 2020

Keywords:
Stirring hydrothermal
Anatase TiO_2
Discharge capacity
Electrochemical

ABSTRACT

Ab-initio, anatase titanium dioxide (TiO_2) nanotubes were prepared from pristine anatase titanium dioxide (TiO_2) nanoparticles via a low temperature modified stirring-hydrothermal technique. Scanning electron microscope (SEM) characterization of the as-synthesized sample depicted uniformly distributed one-dimensional nanotubular morphology, with an average length, thickness and diameter of ~4 μm, 17 nm and 20 nm, respectively. N_2 physisorption of the sample revealed two distinct peaks at mesopore and macropore scales of 3 nm and 100 nm, respectively. The specific surface area of the materials was observed to have increased from 8 $m^2\ g^{-1}$ for the pristine to 62 $m^2\ g^{-1}$ for the nanotubes. X-ray diffraction analysis indicated a tetragonal symmetry for the anatase TiO_2nanotubes sample, which is similar to those reported in the literature. Core levels and elemental analyses showed the presence of titanium and oxygen in good proportion. Electrochemical performances of the TiO_2nanotubes electrode offered good cyclic stability, good rate capability and a fairly large capacity of 160 mA h g^{-1} at a specific current of 36 mA g^{-1}.

1. Introduction

The preparation of TiO_2 nanotubes by a simple hydrothermal technique has been adopted by many researchers in recent years due to its various applications in lithium-ion batteries (Luo et al., 2012), solar cells (Ye et al., 2013), photo catalysts, Bagheri and Julkapli (2016) and biomedical applications (Li et al., 2015). Titania nanotubes can be produced by multiple methods such as replication, template, and anodic oxidation among others. The simple hydrothermal method involves the transformation of a titania particle precursor in sodium hydroxide into nanotubes or nanowires at high temperature, which can be reproducible, having the same composition and dimensions (Kasuga et al., 1998; Kasuga, 2006; Kasuga et al., 1999). TiO_2 nanotubes are formed through the influence of synthesis conditions such as temperature, TiO_2 precursor, reaction time, stirring rate and washing process (Nwankwo et al., 2019; Drozd et al., 2019; de Mendonça et al., 2019; Wang et al., 2012; Rubio et al., 2019). The structural evolution mechanism during hydrothermal treatment process starts immediately the Ti-O-Ti bonds of TiO_2 precursor break and a six-coordinated monomer $[Ti(OH)_6]_2$ is formed and saturated (Zhang et al., 2019). Then, the thin nanosheets start growing leading to formation of 1D $Na_2Ti_3O_7$ nanostructures. $Na_2Ti_3O_7$ nanotubes synthesis occurs at lower temperature due to hydrogen deficiency at the surface of nanosheets, which increases surface tension and causes the surface layer to bend. When the $Na_2Ti_3O_7$ nanotubes are subjected to hydrogen exchange with diluted HNO_3 (0.1 M), the Na^+ ions in the anatase TiO_2 matrix were replaced by H_3O^+ ions to form $H_2Ti_3O_7$ nanotubes. An oriented attachment mechanism of the mechanical force-driven stirring process also enhanced the growth of the titanate nanotubes produced via this method. The anatase TiO_2 (bulk) even at its virgin state, is a good material with exceptional qualities for the anode of lithium-ion batteries, but its main drawback is the poor chemical diffusivity of lithium (Liang et al., 2016). To address the challenge, storage charge of the pristine anatase TiO_2 is subjected to transformation from battery-type to pseudocapacitive charge storage, thereby improving the electrochemical performance of the material. A battery-type electrode exhibits a characteristic cyclic voltammetry profiles with distinct redox peaks separated by a negligible capacitive envelope that does not contribute to the stored charge. For a pseudocapacitive electrode, the stored charge does not remain constant in a specified potential window but

* Corresponding author.
E-mail address: Ncholu.Manyala@up.ac.za (N. Manyala).

https://doi.org/10.1016/j.egyr.2020.02.010

becomes more pronounced at certain potential while the charge storage mechanism is still faradaic by nature (Mathis et al., 2019).

In recent times, nanomaterials with different morphologies /aspect ratios have attracted elevated attention from many researchers. Such materials as one-dimensional (1D) nanostructures, which include belts, wires, fibres, rods, and tubes amongst others due to their electrical properties been dependent on directionality (Reddy et al., 2010). These 1D nanostructures have been synthesized via lithographic process and wet chemical techniques, on a laboratory scale. Nevertheless, these procedures limit the materials finite lengths to several microns. Thus, materials fabrication as continuous nanotubes/fibres via other methods such as stirring hydrothermal is of enhanced interest. TiO_2 nanowire membranes grown on the surfaces of Ti metal by a hydrothermal treatment process using 12 M NaOH aqueous solution at 160 °C for 24 h, displayed a more significant effect on the photocatalytic activity of the resulting TiO_2 nanowires compared to the calcination process (Chang et al., 2017). The TiO_2 in this study in comparison to some literature studies on anatase TiO_2 and other metal oxides such as NiO-Co_3O_4, $NiCo_2O_4$, and CuO-CO_3O_4, shows slight differences in particle size and morphology dependent charge storage mechanism (Reddy et al., 2010; Kunwar et al., 2019). The 1D anatase TiO_2 nanotubes in this work possessed improved performance as anode for lithium ion batteries compared to the nanobelts and nanoparticles earlier reported in the literature (Reddy et al., 2010). The excellent performance stability as well as improved rate capability, beside the satisfying specific capacity of ∼160 mAh g^{-1} obtained at a specific current of 36 mA g^{-1} for the TiO_2 nanotubes compared well to some similar materials earlier reported in the literature (Wang et al., 2012; Reddy et al., 2010; Tang et al., 2014; Wei et al., 2013; Savva et al., 2018; Choi et al., 2010; Gentili et al., 2012).

The electrochemical properties of anatase TiO_2 can be improved by increasing its surface area and changing its state from particles into nanotubes (battery-type into pseudocapacitive behaviour, respectively) via the stirring hydrothermal method as earlier reported (Tang et al., 2014).

The modified stirring hydrothermal technique adopted for the preparation of anatase titanium dioxide nanotubes is similar to the work reported in reference 10 above. Anatase TiO_2 powder was used as starting material to prepare anatase TiO_2 nanotubes instead of P25 TiO_2(B) powder that was reported in the literature. This material was selected because of its stability, and it is relatively cheaper compared to all other types of TiO_2 materials that had been adopted in the literature. Most importantly in the electrochemistry measurement, an increase in the initial capacity and an excellent reversible capacity at 100th cycle showed the uniqueness of the prepared anatase TiO_2 nanotubes for the fabrication of an anode of lithium-ion battery. The intercalation of lithium-ions in TiO_2 anode occurs at about 1.5 V and the chemical equation in the electrochemical processes is given by $TiO_2 + x(Li^+ + e^-) \leftrightarrow Li_xTiO_2$. Anatase TiO_2 has theoretical capacity of 170 mAh g^{-1}, almost equal to $Li_4Ti_5O_{12}$ (LTO), which is 175 mAh g^{-1} (Tang et al., 2014; Wei et al., 2013; Kebede et al., 2016).

Herein, the pristine anatase TiO_2 and TiO_2 nanotubes were successfully investigated as negative electrode (anode) for lithium-ion battery. The growth of nanotubular structure of the TiO_2 is very important to the inclusion and exclusion of lithium ions in lithium ion batteries. It is interesting to note that the pristine anatase TiO_2 showed purely battery-type charge storage mechanism while as-prepared anatase TiO_2 nanotubes exhibited pseudocapacitive charge storage process but the faradaic reaction and diffusion control kinetics occur in the charging–discharging mechanism of both samples.

2. Experimental procedure

0.5 g of Anatase TiO_2 (MercKGaA) powder was added into 30 mL of 10 M sodium hydroxide (NaOH) solution followed by stirring continuously for 2 h to obtain a homogeneous mixture. The mixture was turned into 40 mL autoclave with a magnetic stirrer. Then the autoclave was sealed and gently put in a beaker containing silicon oil, which was eventually place on a hot plate pre-set at a temperature of 130 °C, the stirrer speed was 550 rpm for 24 h. The centrifuge was used to wash the product in deionized water, until the pH value of 9 was obtained. Finally, the residue in form of gel was collected and washed in diluted Nitric acid (0.1 M) and later in distilled water, until the pH value was reduced to 7 (neutral). The equation of the reaction is given below:

$$3TiO_2 + 2NaOH \rightarrow Na_2Ti_3O_7 + H_2O \quad (1)$$

$$Na_2Ti_3O_7 + 2HNO_3 \rightarrow H_2Ti_3O_7 + 2NaNO_3 \quad (2)$$

$$H_2Ti_3O_7 \rightarrow 3TiO_2 + H_2O \quad (3)$$

The recovered sample was oven dried at 60 °C for 24 h in ambient condition. The final product was annealed at 400 °C at a ramping rate of 5 °C/min for 4 h to produce the anatase nanotubular TiO_2 as shown in Fig. 1.

2.1. Characterization of pristine and prepare anatase TiO_2

The surface of the pristine and prepared anatase samples was observed by using a Zeiss Ultra Plus 55 field emission scanning electron microscope (FE-SEM) operated at 2.0 kV and JEM-2100F transmission electron microscope (TEM). The elemental analyses were also determined by using energy dispersive x-ray (EDX) Oxford instruments (Aztec 3.0 SP1 software) attached to the SEM. The surface areas and porosities of the samples were measured with Brunauer–Emmett–Teller (BET), the pristine and prepared TiO_2 nanotubes were characterized by using X-ray diffraction (XRD) on a XPERT-PRO Diffractomer with a cobalt target (λ = 1.7890 Å). Core level measurements were carried out using X-ray photoelectron spectroscopy (XPS). The XPS measurements of the samples were conducted using a Physical Electronics VersaProbe 5000 spectrometer operating with a 100 mm monochromatic Al-Ka exciting source.

2.2. Fabrication of half-cell device

The electrodes of pristine TiO_2 and TiO_2 nanotubes were produced by mixing 80% active material powder (pristine TiO_2 or prepared TiO_2 nanotubes) with 10% binder (polyvinylidene fluoride), 10% conductive carbon black and drops of N-methyl-2-pyrrolidone, then mixed for 2 h. The doctor blade was used to coat the mixture (slurry) on copper foil current collector. The film was allowed to dry in a vacuum at 100 °C overnight to ensure an oxygen-free environment for complete adherence of the film to the copper substrate. The dried film was punched into a 16 mm diameter disc, with active material loading-mass of ∼3.5 mg cm^{-2}. The prepared electrode was then transferred into an argon-filled glovebox with moisture and oxygen levels maintained at less than 1 ppm for assembly as anode material, with a separator made of polypropylene (Celgard 2400), lithium foil as reference/counter electrode and an organic electrolyte, 1M $LiPF_6$ solution in the mixture of ethylene carbonate and dimethyl carbonate (EC/DEC 1:1 in volume). The lithium foil, separator and anode material were impacted by a metallic spacer for firm contact in a 2032 grade coin cell. Galvanostatic measurements of the materials were performed to understand the charge/discharge behaviour of the half-cell electrodes using a

Fig. 1. A set-up of stirring hydrothermal for the growth of TiO_2 Nanotubes.

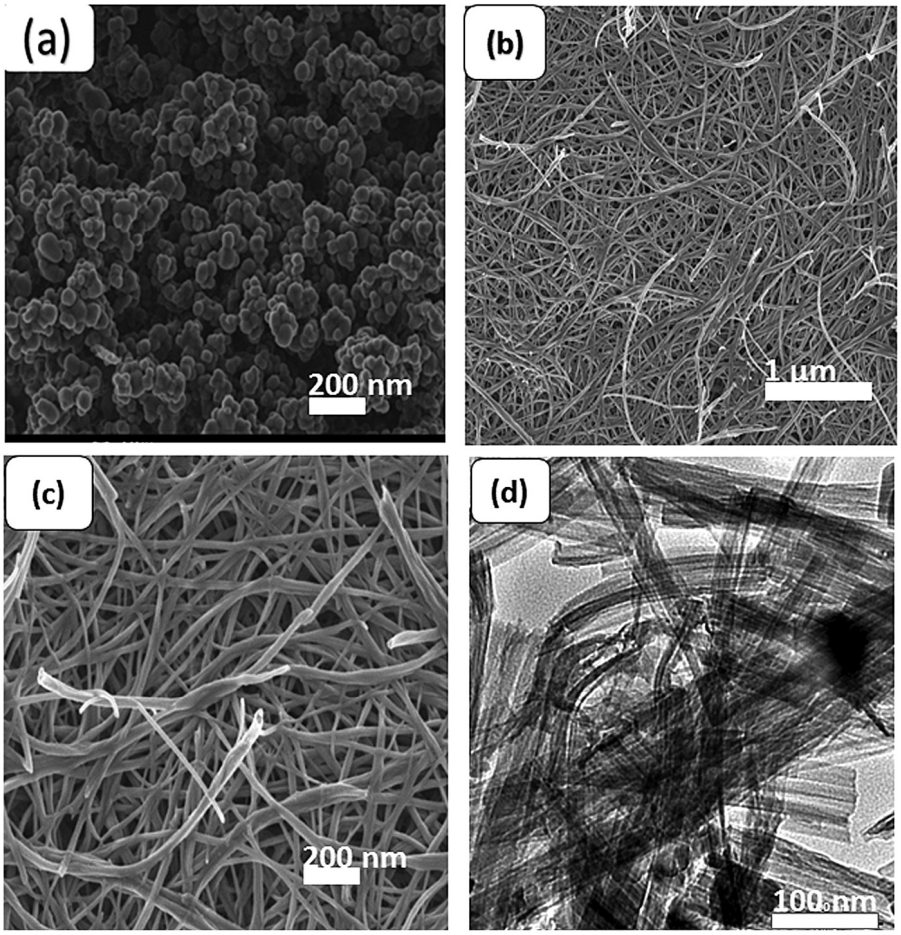

Fig. 2. (a) Anatase pristine TiO_2 powder micrograph (SEM) at high magnification, (b and c) Anatase TiO_2 nanotubes micrographs (SEM) at different magnifications and (d) TEM micrograph of anatase TiO_2 nanotubes at high magnification.

MACCOR series 4000 battery testing station, while the electrochemical impedance spectroscopy (EIS) analysis were performed using a VMP300 Bio-Logic potentiostat/galvanostat controlled by EC-Lab v10.40 software at a frequency range between 100 kHz and 10 mHz and cyclic voltammetry (CV) measurements were carried out at a scan rate of 0.1 mV s^{-1} in the potential window of 1.0 to 3.0 V vs. Li/Li^+ on a VMP300 Bio-logic facility.

3. Results and discussion

3.1. Surface and structural analyses

Fig. 2a shows the morphology of pristine TiO_2 powder at high magnification as agglomerated nanoparticles. Fig. 2(b and c) shows the morphology of the anatase TiO_2 nanotubes at different magnifications. It was observed that the nanoparticles and nanotubes are uniformly distributed, depicting stone-like shape for the pristine material, and nanotubular shape for the prepared material, respectively. Therefore, the results showed that very long and evenly distributed nanotubes were successfully prepared. This corroborated the fact that there is an increase in the specific surface area of prepared material as revealed by the BET results (Fig. 3b). Fig. 2(c) displays the micrograph of the nanotubes at a higher magnification. The one dimensional (1D) hollow tubes were interconnected, which could enhance the intercalation and de-intercalation of lithium-ion in the electrode. Figure S3 in the supporting information depicts the SEM morphology of the anode

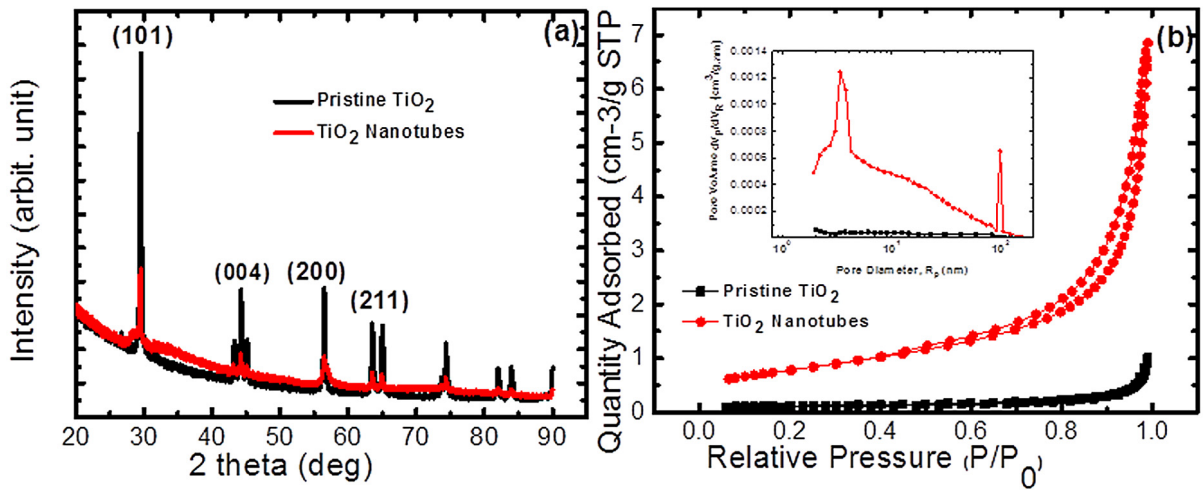

Fig. 3. (a) XRD patterns of pristine TiO_2 and TiO_2 nanotubes and (b) Nitrogen desorption isothermal pattern of the anatase pristine TiO_2 and prepared anatase TiO_2 nanotubes at 130 °C for 24 h (inset of the graph shows the pore size distribution).

material after a cycling test of over 100 cycles. It could be observed that the electrode's morphology remained the same even after the long cycling test of over 100 cycles, indicating durability of the anode material after high cycling stability.

The TEM sample was prepared by adding the prepared material in high concentration ethanol (99%) and subjected it to ultrasonic treatment, dropping the solution onto on a copper substrate (grid) and then allowed to dry in the air. Fig. 2(d) showed agglomerated nanotubes with an average value of ∼20 nm, 3 nm and 4 μm for external diameter, internal diameter and length, respectively. The average thickness of the nanotube was estimated to about 17 nm.

Fig. S1 in supporting information shows the elemental analysis of the TiO_2 nanotubes with that of plane epoxy resin (inset) used as substrate in sample preparation for analysis. Also as inset to Figure S1 is a table showing both the sample and epoxy resin compositional elements (at wt.%). The EDX spectra show the presence of Ti and O as major elements in the sample. A trace of Na (0.09 wt%) observed in the spectrum could be attributed to the high concentration sodium hydroxide used in sample preparation, while C is due to the graphite coating employed in sample preparation for the EDX analysis. Si and Cl recorded in the spectra are present due to the epoxy resin adopted as substrate in sample preparation for the EDX analysis, and are not in any way part of the sample used for electrode (Anode) fabrication. Thus, they do not affect the final electrochemical properties.

Fig. 3a represents the patterns of XRD for anatase pristine TiO_2 and TiO_2 nanotubes carried out via a XPERT-PRO diffractometer at 2θ values (20–90°), using a Co-Kα radiation source ($\lambda = 1.7890$ Å) at 50 kV and 30 mA. The figure shows the corresponding first four diffraction peaks indexed at 29.43(101), 44.07(004), 56.35(200), 64.84(211) planes (Taleatu et al., 2016) belonging to tetragonal structure. The peaks were identified as anatase TiO_2 peaks (COD: 01-071-1167) which crystallized in the tetragonal symmetry with space group $I4_1/amd$ and lattice parameters $a = b = 3.7892$ Å, c = 9.5370 Å. The (101) peak was clearly identified, and confirmed the presence of anatase phase. The rutile and brookite phases are completely absent in the prepared samples.

The BET analysis revealed the absorption and desorption properties of the samples as shown in Fig. 3b. The inset of the graph shows the pore size distribution of both samples. The nitrogen desorption isothermal patterns of the pristine and prepared TiO_2 nanotubes possessed type III behaviour with H3-type hysteresis (Alothman, 2012). The absorbent pores categorized the materials into three major classes: micropore (diameter < 2 nm), mesopore (diameter 2–50 nm) and macropore (diameter >50 nm) (Ryu et al., 1999). The prepared material revealed the porosity as mesopores (3 nm) and macropores (100 nm) by the pore size distribution of anatase TiO_2 nanotubes. Anatase TiO_2 nanotubes with the high surface area, 62 $m^2\ g^{-1}$ was revealed, which is preferred over pristine anatase TiO_2 (8 $m^2\ g^{-1}$) for lithium ion battery.

3.2. Core level and elemental analysis

The X-ray photoelectron spectroscopy spectra of Ti2p, O1s and C1s in pristine TiO_2 and prepared TiO_2 nanotubes samples are presented in Fig. 4(a–b), (c–d) and (e–f), respectively. Fig. S2 (see supplementary information) showed the survey spectra that confirmed all elements that are present in the samples by revealing the presence of Titanium, Carbon and Oxygen. The small amount of carbon element observed emanated from carbon tape used during the sample preparation. The observed position of Binding Energy of each element and other parameters such as spectra of full-width-at-half maximum and area were varied within the reference based interval. Fig. 4(a–b) showed the spectra of Ti2p of pristine anatase TiO_2 and TiO_2 nanotubes respectively. The positions of Binding Energy (B.E.) of $2p_{3/2}$ were almost the same in both samples, while the position of $2p_{1/2}$ varied. However, photoelectron peaks of pristine material at B.E position of 455.91 eV and 461.62 eV were observed with spin–orbit splitting of about 5.71 eV. The peaks of nanotubular TiO_2 are located at B.E position of 455.95 eV and 462.22 eV having spin–orbit splitting of about 6.27 eV. The two spin–orbits splitting (5.71 eV and 6.27 eV) acquired were consistent with the line of Ti2p doublet core level found in TiO_2 structure. This is in tandem with the work reported in the earlier study (Zhang et al., 2019). The B.E positions of $2p_{1/2}$ peaks were shifted slightly after the preparation of nanotubes and this may be due to the change in chemical state. The change in binding energy to lower values may have actually resulted from the formation of oxygen vacancies due to the breaking of Ti-O-Ti bonds in the TiO_6 octahedrons when the TiO_2 was subjected to alkaline treatment in NaOH medium (Arruda et al., 2015). Thus, the chemical shift in binding energies is linked to $Ti2p_{1/2}$ peak in the stoichiometric Titanium dioxide (TiO_2) structure. Oxygen vacancies in the annealed TiO_2 nanotube electrode could cause a defect that leads to an increase in electronic conductivity of the material and thereby responsible for the enhanced lithium storage properties (Savva et al., 2018). The oxygen vacancies

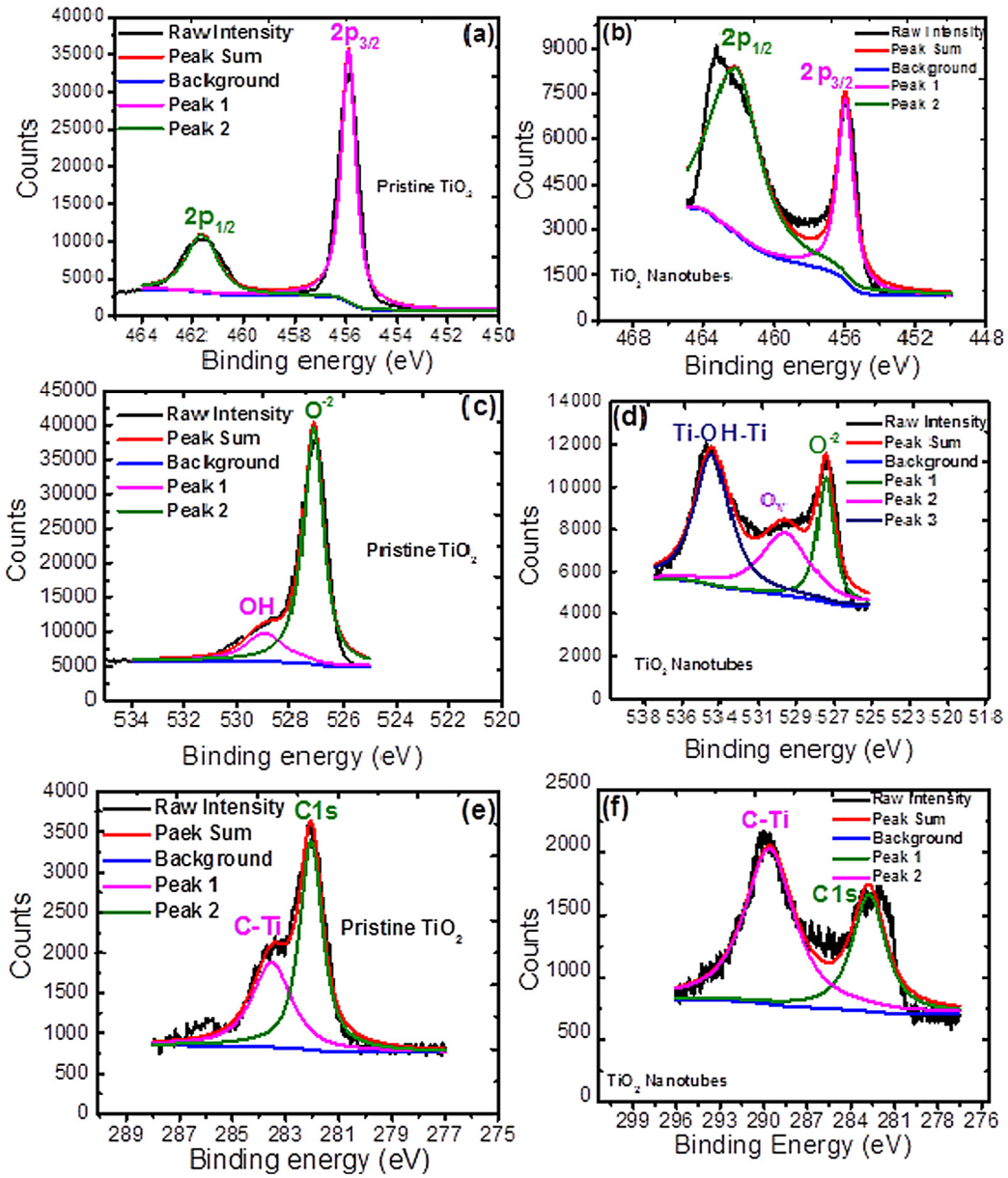

Fig. 4. XPS spectra of (a–b) Ti2p (c–d) O1s (e–f) C1s for pristine TiO_2 and TiO_2 Nanotubes, respectively.

could stretch lattice spaces, further reduce charge transfer resistance, and supply more active sites in the TiO_2 nanotubes lattices, resulting in a fairly large reversible capacity of 160 mAh g^{-1} at a specific current of 36 mA g^{-1}. The controlled oxygen vacancies as well as the nanorods morphology in the heat treated TiO_2 anodes are attributed to the improved lithium storage properties of the material.

However, the spectra of oxygen components were clearly shown in Fig. 4(c–d) which were subjected to deconvolution and split into two and three peaks, respectively. The B.E positions of the peaks for pristine sample were identified at 527.15 eV and 528.93 eV, representing surface (OH) and bulk oxygen (O^{-2}), respectively (Geogios and Wolfgang, 2010). Likewise, The B.E positions of the peaks for TiO_2 nanotubes could be identified by three components located at 527.49 eV, 529.86 eV and 530.5 eV, attributed to absorbed oxygen atoms in water molecules, lattice oxygen atoms, and oxygen vacancies (O_V), respectively, indicating that oxygen vacancies were further generated during the annealing treatment of the material. The removal of oxygen atoms in the lattice sites to the gaseous state could generally lead to formation of oxygen vacancies. The contact of water molecules with nanotube surface, absorbed at the bridging oxygen vacancies can lead to Ti-OH-Ti bridge (Preethi et al., 2017). It should be noted that the hydroxylic solution (NaOH) has been successfully used as an alkaline medium to grow TiO_2 nanotubes. There was a difference in the peak area of pristine TiO_2 and TiO_2 nanotubes that can be attributed to the atoms as a result of trapped environmental moisture and free hydroxyl group (Biswas et al., 2006). The binding energy of each spectrum of C1s was fixed at 282.04 eV and 283.52 eV as reference in the pristine material as shown in Fig. 4e, while Fig. 4f (TiO_2 nanotubes) revealed a second peak at 289.7 eV, this value is assigned to the bond of carbon to another metal, like Ti or Na (Roy et al., 2005). This carbon can be chemically bonded as C-O-Ti or C-O-Na. Table S1 (a–b) gives detailed parameters of XPS spectra, which can be found in the supporting information.

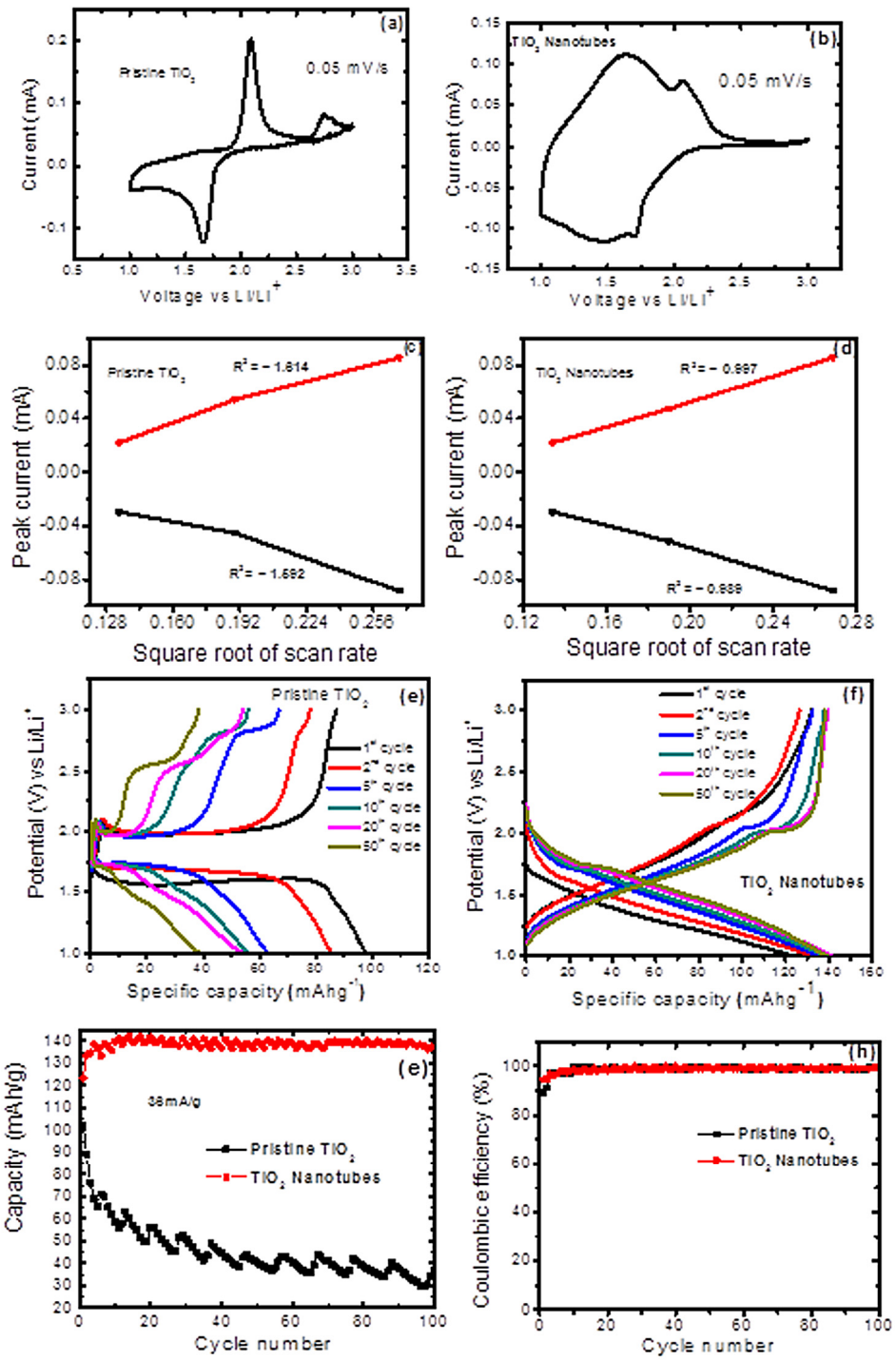

Fig. 5. (a–b) Cyclic Voltammetry curves of pristine TiO_2 and prepared TiO_2 nanotubes, (c–d) plot of anodic and cathodic peak current against square root of the scan rate for pristine TiO_2 and TiO_2 nanotubes, (e–f) CD curves of pristine TiO_2 and prepared TiO_2 nanotubes, (g) Performance of prepared TiO_2 nanotubes and pristine TiO_2 at 36 mA g^{-1} in the 1–3 V potential window and (h) Columbic efficiency against cycle number of prepared TiO_2 nanotubes and pristine TiO_2.

3.3. Electrochemical analysis

The electrochemical test of the pristine TiO_2 and TiO_2 nanotubes were performed in a half-cell configuration. Fig. 5(a, b) showed cyclic voltammetry (CVs) of the pristine anatase TiO_2 and prepared TiO_2 nanotubes scanned at a rate of 0.05 mV s^{-1} in a potential window of (2.0 V) 1.0–3.0 V vs. Li/Li^+. In the pristine TiO_2 powder, the anodic/cathodic peaks were located at 2.09/1.66 V respectively as shown in Fig. 5a. The anatase TiO_2 nanotubes showed major peaks at 1.61/1.70 V for anode/cathode respectively, while the minor anodic/cathodic peaks were also located at 2.05/1.52 V. The electrolytic lithium insertion and extraction associated with peaks of the anatase structure for anodic and cathodic parts were 2.05/1.70 V respectively (Gao et al., 2005; Kavan et al., 2004; Subramanian et al., 2006; Zhao et al., 2007; Choi et al., 2010). The TiO_2 Nanotubes exhibited pseudocapacitive charge storage behaviour similar to previous reports (Mathis et al., 2019; Choi et al., 2010). Fig. 5(c and d) displays a linear relationship of the peak specific current as a function of the square roots of scan rate, which was estimated

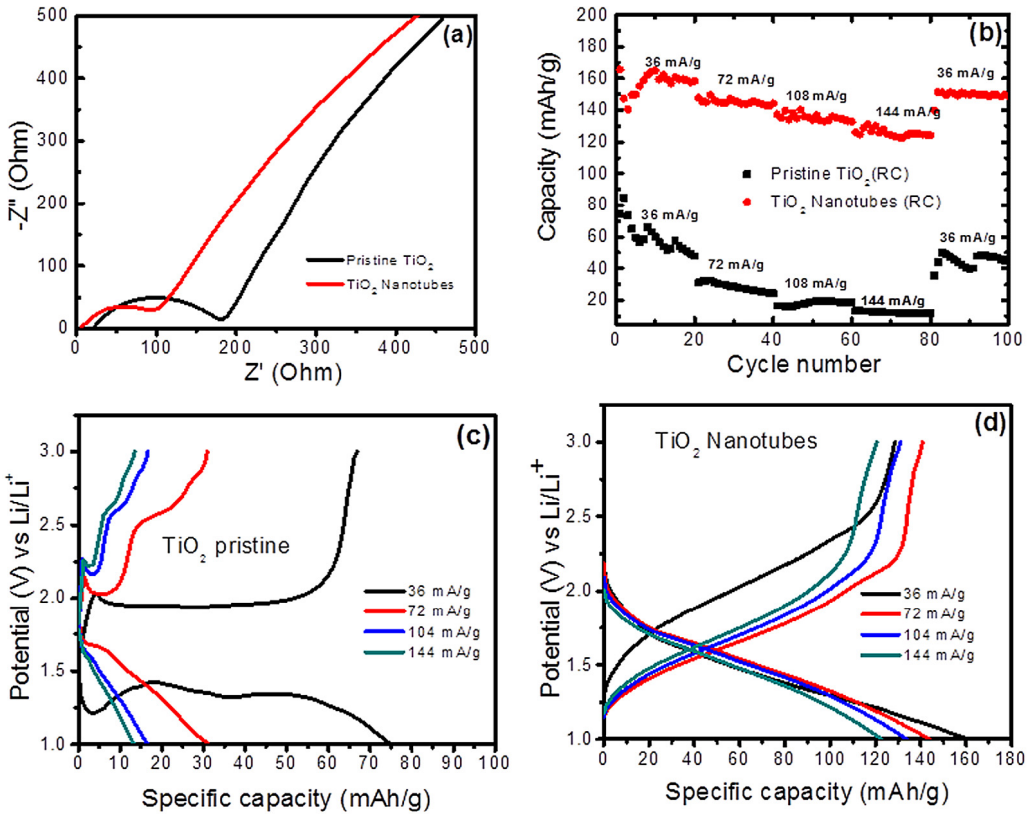

Fig. 6. (a) The plot of Nyquist graph clearly showing the reduction in the values of resistance (R_{ct} and R_s) for both pristine and prepared TiO_2 nanotubes, (b–d) Rate capability of pristine and prepared TiO_2 nanotubes at current density ranging from 36 to 144 mA g^{-1} in the potential window of 1–3 V.

by using the Origin Pro 9.0 software. From Fig. 5b, the linearity of the plots confirmed that the electrochemical reaction is diffusion controlled, and further affirms the swift Faradaic charge storage process within the TiO_2 nanotubular material electrode compared to the non-linear relationship observed for the pristine TiO_2 material in Fig. 5c, which demonstrates the pristine material is not diffusion controlled. Fig. 5(e–f) shows the galvanostatic charge–discharge tests performed on the samples in a potential range of 1.0–3.0 V at various specific currents. Two potential plateaus were noticed at 1.75 V and 2.0 V for the pristine and nanotubes materials, indicating discharging and charging which correspond to insertion and de-insertion of lithium-ion, respectively (Wagemaker et al., 2007). The three different assumptions for the insertion of lithium mechanism in the voltage region of 1–1.75 V were the formation of a Li-rich $Li_{0.5} + xTiO_2$ in the tetragonal lattice, Wagemaker et al. (2007), Borghols et al. (2009, 2010), Ren et al. (2010) reversible interfacial lithium storage, Ren et al. (2010), Shin et al. (2011), Jamnik and Maier (2003), Wang et al. (2007) and lastly the electrolytic composition and depletion of a solid electrolyte interphase (Aurbach et al., 1999).

The pristine material gave a specific capacity of only 98 mAh g^{-1} at first cycle, but drastically reduced to 38 mAh g^{-1} at 100th cycle as clearly shown in Fig. 5g. On the other hand, the prepared nanotubes exhibited an unprecedented property of electrochemical performance, displaying an increase value of capacity of about 123 mAh g^{-1} at first cycle to 142 mAh g^{-1} at 100th cycling performance. The capacity loss relative to the initial discharge capacity for the pristine electrode at 100th cycle is about 66%, while the nanotubular TiO_2 electrode showed about 17% increase from its initial value at 100th cycles (Fig. 5g). This result showed a remarkable improvement on the prepared TiO_2 nanotubes which exhibited no capacity fade, but rather showed an increase in the value of discharge capacity. The electrode rarely exhibited such a strange property as an anode of a lithium ion battery. This strange behaviour could be attributed to the fact that the prepared nanotubes provide direct and rapid ion pathways and also glue to one another to form a mechanical stability of cross-linked network due to their flexible nature (Tang et al., 2014). The ratio of discharge to charge capacity is referred to cycling efficiency, it is always lesser than 1 and the coulombic efficiency is simply its percentage. Fig. 5h compares the pristine TiO_2 with the prepared TiO_2 nanotubes in terms of their efficiencies. The figure clearly showed fluctuations in the pristine material which made it unstable but became very stable for TiO_2 nanotubes during 100th cycles and this could possibly indicate that the nanotubes play a vital role in binding the electrode together, and allowing it to expand and contract reversibly with lithiation and delithiation. Hence, the excellent performance stability and rate capability of the TiO_2 Nanotubes shown in Fig. 5g and h displayed better performances than the work reported by Choi et al. (2010) and Gentili et al. (2012).

The electrochemical impedance spectroscopy (EIS) of the samples was conducted in an open-circuit potential and in a frequency range of 10 mHz to 100 kHz. The EIS tests were performed to determine the electrical properties of the cells. The Nyquist plot for pristine and prepared TiO_2 nanotubes is as shown in Fig. 6a. The extrapolation of solution resistance (R_s) and was determined from Fig. 6a and reported in Table 2. The intrinsic resistance of the pristine anatase TiO_2 or prepared anatase TiO_2 nanotubes, current collector (lithium metal) and ionic resistance of the electrolyte contributed to the value of solution resistance (R_s) while the charge interfacial charge and mass movement within the material were determined by charge-transfer resistance (R_{ct}) (Jagadale et al., 2016; Luo et al., 2013). Thus, the reduction in the charge transfer resistance value translated to an increase in the cell capacity. It should also be noted here

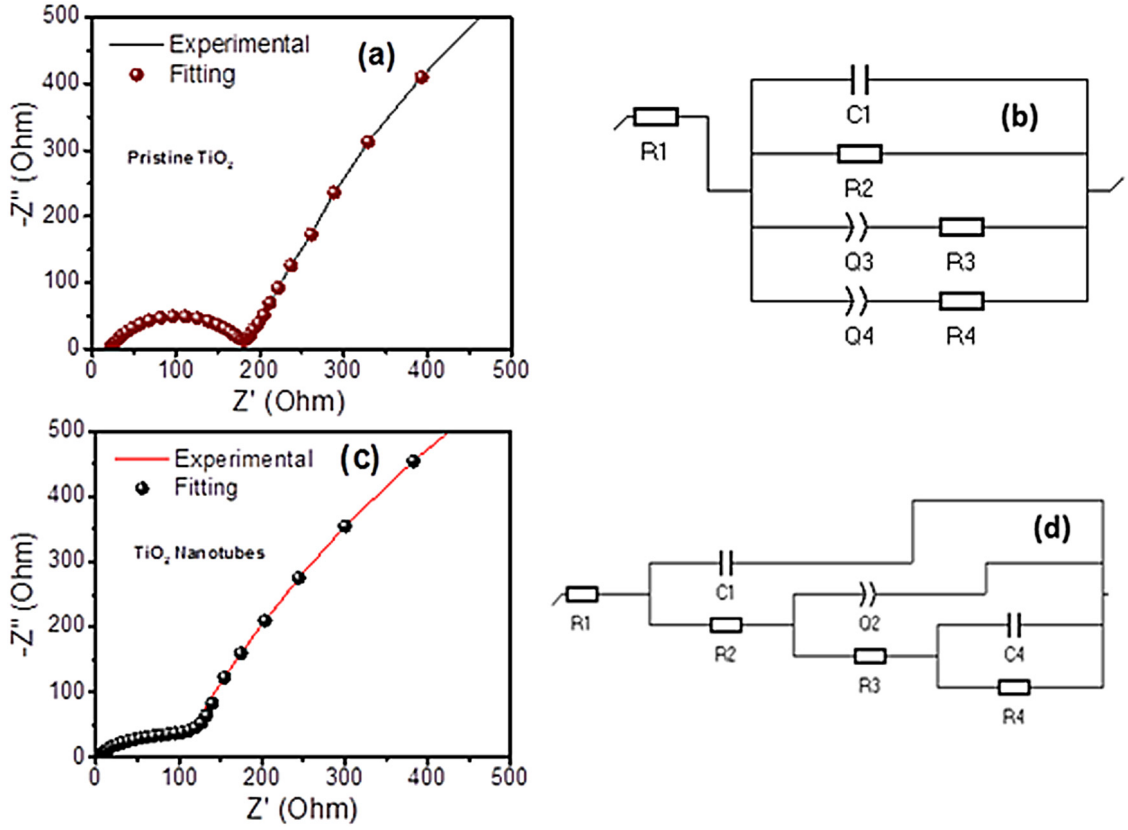

Fig. 7. (a–b) Fitted Nyquist plot and its equivalent circuit model for pristine TiO_2 and (c–d) fitted Nyquist plot and its equivalent circuit model for TiO_2 nanotubes, respectively.

that the anatase TiO_2 nanotube has lower ionic and electronic resistance compared to that of pristine electrode, which contributed to its higher and outstanding rate capability as shown in Fig. 6b, hence the kinetics of lithium insertion/de-insertion rate of the nanotubular electrode is faster and the rate capability drops slightly at higher discharge specific currents. The voltage profiles of the electrode of pristine and prepared TiO_2 nanotube half-cells were shown in Fig. 6c and d respectively, showing a very limited increase of the cell polarization upon increasing the specific current density for TiO_2 nanotubes but behaved poorly with pristine material. The exchanged capacity ranges between 160 to 122 mAh g^{-1} at 36 mA g^{-1} and 144 mAh g^{-1} respectively. The rate capability of anatase TiO_2 nanotubes was much better than the pristine material. The detailed capacities of the pristine and nanotubular materials are reported in Table 1.

Table 2 showed a summary of the parameters from the EIS analysis for both the TiO_2 pristine and TiO_2 nanotubes materials respectively. Hence, the electrode of anatase TiO_2 nanotubes was observed to display much more improvement in terms of electrochemical performance than the pristine anatase TiO_2. Fig. 7(a–d) showed fitting and EIS plots with their equivalent circuit models for pristine and nanotubular TiO_2. Briefly, R_1, R_2 and C_1 are equivalent to solution resistance (R_s), charge transfer resistance (R_{ct}) and double layer capacitance (C_{DL}), respectively.

Table 1
Discharge capacity of pristine TiO_2 and TiO_2 nanotubes at various current densities.

Current density (mA g^{-1})	Pristine TiO_2, 1st cycle capacity (mAh g^{-1})	TiO_2-NT, 1st cycle capacity (mAh g^{-1})
36	75	160
72	32	144
108	17	132
144	14	122

Table 2
Resistance values of the half-cell devices.

Device parameters	R_s (Ω)	R_{ct} (Ω)
Pristine TiO_2	22.07	167.93
TiO_2 nanotubes	5.77	121.97

4. Conclusion

The study reported the preparation of TiO_2 nanotubes from anatase TiO_2 powder via modified stirring hydrothermal technique. Thus, the characterization of both materials (Pristine TiO_2 and TiO_2 nanotubes) showed that the prepared TiO_2 nanotubes exhibited better anodic properties suitable for the design of a lithium-ion battery. Hence, the pristine and prepared materials were tested as anodes in the lithium ion batteries using a half-cell configuration. The electrochemical behaviour of the anatase TiO_2 nanotubes showed a stable anodic material compared with pristine TiO_2 result after cycling up to 100 cycles. However, the value of about 17% increase from the initial value of discharge capacity at 100th cycles was observed for anatase TiO_2 and the rate capability of the prepared anatase TiO_2 nanotubes upon increasing the specific current density was excellent compared with the pristine material. The nanotubular electrode exhibited a reduction in the value of resistance, which translated to a better electrochemical performance in the anode of lithium ion battery.

Declaration of competing interest

The authors declare that they have no known competing financial interests or personal relationships that could have appeared to influence the work reported in this paper.

CRediT authorship contribution statement

O. Fasakin: Conceptualization, Data curation, Formal analysis, Methodology, Writing - original draft, Writing - review & editing. **Kabir O. Oyedotun:** Data curation, Formal analysis, Methodology, Writing - original draft, Writing - review & editing. **Mesfin Kebede:** Formal analysis, Resources, Methodology, Writing - original draft. **Mark Rohwer:** Formal analysis, Writing - original draft. **Lukas Le Roux:** Formal analysis, Methodology, Writing - original draft. **Mkhulu Mathe:** Formal analysis, Resources. **M.A. Eleruja:** Formal analysis, Supervision, Writing - original draft. **E.O.B. Ajayi:** Formal analysis, Supervisor, Writing - original draft. **Ncholu Manyala:** Conceptualization, Supervision, Formal analysis, Writing - review & editing.

Acknowledgements

The South African Research Chairs Initiative (SARChI) of the Department of Science and Technology in conjunction with the National Research Foundation (NRF) of South Africa (Grant No. 61056) supported this research work. The authors declare no conflict of interest. Dr Fasakin O. deeply appreciates Obafemi Awolowo University, Ile-Ife for granted leave.

Appendix A. Supplementary data

Supplementary material related to this article can be found online at https://doi.org/10.1016/j.egyr.2020.02.010.

References

Alothman, Z.A., 2012. A review: fundamental aspects of silicate mesoporous materials. Materials 5, 2874–2902.

Arruda, L.B., Santos, C.M., Orlandi, M.O., Schreiner, W.H., Lisboa-Filho, P.N., 2015. Formation and evolution of tio_2 nanotubes in alkaline synthesis. Ceram. Int. 41, 2884–2891.

Aurbach, D., Markovsky, B., Weissman, I., Levi, E., Ein-Eli, Y., 1999. On the correlation between surface chemistry and performance of graphite negative electrodes for Li ion batteries. Electrochim. Acta 45, 67–86.

Bagheri, S., Julkapli, N.M., 2016. Phosphorene: A new competitor for grapheme. Int. J. Hydrog. Energy 41, 4085–4095.

Biswas, P.K., De, A., Dua, L.K., Chkoda, L., 2006. Surface characterization of sol–gel derived indium tin oxide films on glass. Bull. Mater. Sci. 29, 323–330.

Borghols, W.J.H., Lutzenkirchen-Hecht, D., Haake, U., Chan, W., Lafont, U., Kelder, E.M., van Eck, E.R.H., Kentgens, A.P.M., Mulder, F., Wagemaker, M., 2010. Lithium storage in amorphous tio_2 nanoparticles. J. Electrochem. Soc. 157, A582–A588.

Borghols, W.J.H., Wagemaker, M., Lafont, U., M.Kelder, E., Mulder, F.M., 2009. Size effects in the $li_{4+x}ti_5o_{12}$ spinel. J. Am. Chem. Soc. 131, 17786–17792.

Chang, Y., Wu, C., Wang, H., Xiong, Y., Chen, Y., Ke, K., Hec, Y., Dong, S., 2017. Effect of post-heat treatment on the photocatalytic activity of titanium dioxide nanowire membranes deposited on a ti substrate. RSC Adv. 7, 21422.

Choi, M.G., Lee, Y., Song, S., Kim, K.M., 2010. Lithium-ion battery anode properties of tio_2 nanotubes prepared by the hydrothermal synthesis of mixed (anatase and rutile) particles. Electrochim. Acta 55, 5975–5983.

Drozd, V.S., Zybina, N.A., Abramova, K.E., Parfenov, M.Y., Kumar, U., Valdés, H., Smirniotis, P.G., Vorontsov, A.V., 2019. Oxygen vacancies in nano-sized tio_2 anatase nanoparticles. Solid State Ion. 339, 115009.

Gao, X.P., Lan, Y., Zhu, H.Y., Liu, J.W., Ge, Y.P., Wu, F., Song, D.Y., 2005. Electrochemical performance of anatase nanotubes converted from protonated titanate hydrate nanotubes. Electrochem. Solid State Lett. 8, A26–A29.

Gentili, V., Brutti, S., Hardwick, L.J., Armstrong, A.R., Panero, S., Bruce, P.G., 2012. Lithium insertion into anatase nanotubes. Chem. Mater. 24, 4468–4476.

Geogios, P., Wolfgang, S.M., 2010. X-ray photoelectron spectroscopy of anatase-tio_2 coated carbon nanotubes. In: Solid State Phenomena, Vol. 162. pp. 163–177.

Jagadale, A.D., Guan, G., Li, X., Du, X., Ma, X., 2016. Ultrathin nanoflakes of cobalt–manganese layered double hydroxide with high reversibility for asymmetric supercapacitor. J. Power Sources 306, 526–534.

Jamnik, J., Maier, J., 2003. Nanocrystallinity effects in lithium battery materials aspects of nano-ionics, part IV. J. Phys. Chem. Chem. Phys. 5, 5215–5220.

Kasuga, T., 2006. Formation of titanium oxide nanotubes using chemical treatments and their characteristic properties. Thin Solid Films 496, 141–145.

Kasuga, T., Hiramatsu, M., Hoson, A., Sekino, T., Niihara, K., 1998. Formation of titanium oxide nanotube. Langmuir 14, 3160–3163.

Kasuga, T., Hiramatsu, M., Hoson, A., Sekino, T., Niihara, K., 1999. Titania nanotubes prepared by chemical processing. Adv. Mater. 11, 1307–1311.

Kavan, L., Kalbá, M., Zukalová, M., Exnar, I., Lorenzen, V., Nesper, R., Grätzel, M., 2004. Lithium storage in nanostructured tio_2 made by hydrothermal growth. Chem. Mater. 16, 477–485.

Kebede, M., Zheng, H., Ozoemena, K.I., 2016. Metal oxides and lithium alloys as anode materials for lithium-ion batteries. nanomaterials. In: Advanced Batteries and Supercapacitors. Springer, pp. 55–91.

Kunwar, R., Harilal, M., Krishnan, S.G., Pal, B., Misnon, I.I., Mariappan, C.R., Ezema, F.I., Elim, H.I., Yang, C., Jose, R., 2019. Pseudocapacitive charge storage in thin nanobelts. Adv. Fiber Mater. 1, 205–213.

Li, H.Q., Lai, Y.K., Huang, J.Y., Tang, Y.X., Yang, L., Chen, Z., Keqin, Z., Xincai, W., Lay, T., 2015. Multifunctional wettability patterns prepared by laser processing on superhydrophobic tio_2 nanostructured surfaces. J. Mater. Chem. B. 3, 342–347.

Liang, K., Chen, X., Guo, Z., Hou, T., Zhang, X., Li, Y., 2016. Lithium intercalation and diffusion in tio_2 nanotubes: a first-principles investigation. Phys. Chem. Chem. Phys. 18, 24370.

Luo, J., Jang, H.D., Huang, J., 2013. Effect of sheet morphology on the scalability of graphene-based ultracapacitors. ACS Nano 7, 1464–1471.

Luo, Y.S., Luo, J.S., Jiang, J., Zhou, W.W., Yang, H.P., Qi, X.Y., Zhang, H., Fan, H.J., Yu, D.Y.W., Li, C.M., Yu, T., 2012. Seed-assisted synthesis of highly ordered tio_2@a-fe_2o_3 core/shell arrays on carbon textiles for lithium-ion battery applications. Energy Environ. Sci. 5, 6559–6566.

Mathis, T.S., Kurra, N., Wang, X., Pinto, D., Simon, P., Gogotsi, Y., 2019. Energy storage data reporting in perspective—Guidelines for interpreting the performance of electrochemical energy storage systems. Adv. Energy Mater. 190200.

de Mendonça, V.R., Lopes, O.F., Avansi Jr, W., Arenal, R., Ribeiro, C., 2019. Insights into formation of anatase tio_2 nanoparticles from peroxo titanium complex degradation under microwave-assisted hydrothermal treatment. Ceram. Int. 45, 22998–23006.

Nwankwo, U., Bucher, R., Ekwealor, A.B.C., Khamlich, S., Maaza, M., Ezema, F.I., 2019. Synthesis and characterizations of rutile-tio_2 nanoparticles derived from chitin for potential photocatalytic applications. Vacuum 161, 49–54.

Preethi, L.K., Anthony, P., Mathew, T., Walczak, L., Gopinath, C.S., 2017. A study on doped heterojunctions in tio_2 nanotubes: an efficient photocatalyst for solar water. Sci. Rep. 7, 14314.

Reddy, M.V., Jose, R., Teng, T.H., Chowdari, B.V.R., S, 2010. Ramakrishna preparation and electrochemical studies of electrospun tio_2 nanofibers and molten salt method nanoparticles. Electrochim. Acta 55, 3109–3117.

Ren, Y., Hardwick, L.J., Bruce, P.G., 2010. Lithium intercalation into mesoporous anatase with an ordered 3D pore structure. Angew. Chem. 122, 2624–2628.

Roy, S.S., McCann, R., Papakonstantinou, P., Maguire, P., Mclaughlin, J.A., 2005. The structure of amorphous carbon nitride films using a combined study of nexafs, XPS and Raman spectroscopies. Thin Solid Films 482, 145–150.

Rubio, S., Maça, R.R., Aragón, M.J., Cabello, M., Castillo-Rodríguez, M., Lavela, P., Tirado, J.L., Etacheri, V., Ortiz, G.F., 2019. Superior electrochemical performance of tio_2 sodium-ion battery anodes in diglyme-based electrolyte solution. J. Power Sources 432, 82–91.

Ryu, Z., Zheng, J., Wang, M., Zhang, B., 1999. Characterization of pore size distributions on carbonaceous adsorbents by DFT. Carbon 37, 1257–1264.

Savva, A.I., Smith, K.A., Lawson, M., Croft, S.R., Weltner, A.E., Jones, C.D., Bull, H., Simmonds, P.J., Li, L., Xiong, H., 2018. Defect generation in tio_2 nanotube anodes via heat treatment in various atmospheres for lithium-ion batteries. Phys. Chem. Chem. Phys. 20, 22537–22546.

Shin, J.Y., Samuelis, D., Maier, J., 2011. Sustained lithium-storage performance of hierarchical, nanoporous anatase tio_2 at high rates: Emphasis on interfacial storage phenomena. J. Adv. Funct. Mater. 21, 3464–3472.

Subramanian, V., Karki, A., Gnanasekar, K.I., Eddy, F.P., Rambabu, B., 2006. Nanocrystalline tio_2 (anatase) for li-ion batteries. J. Power Sources 159, 186–192.

Taleatu, B.A., Omotoso, E., Tessemamola, G., 2016. Surface structure and photoemission studies of nanocrystalline tio_2 layer/ITO coated glass interface. J. Electron Spectrosc. Relat. Phenom. 207, 1–6.

Tang, Y., Zhang, Y., Deng, J., Wei, J., Tam, L.H., Chandran, B.K., Chen, X., 2014. Mechanical force-driven growth of elongated bending tio_2-based nanotubular materials for ultrafast rechargeable lithium ion batteries. Adv. Mater. 26, 6111–6118.

Wagemaker, M., Borghols, W.J.H., Mulder, F.M., 2007. Large impact of particle size on insertion reactions, a case for anatase $li_x tio_2$. J. Am. Chem. Soc. 129, 4323.

Wang, M.J., Li, C.F., Lai, W.J., Yen, S.K., 2012. Characterization of tio_2 thin films prepared by electrolytic deposition for lithium ion battery anodes. Thin Solid Films 520, 6744–6751.

Wang, J., Polleux, J., Lim, J., Dunn, B.J., 2007. Pseudocapacitive contributions to electrochemical energy storage in tio_2 (anatase) nanoparticles. Phys. Chem. C. 111, 14925–14931.

Wei, W., Oltean, G., Tai, C.W., Edström, K., Björefors, F., Nyholm, L., 2013. High energy and power density tio_2 nanotube electrodes for 3D li-ion microbatteries. J. Mater. Chem. A 1, 8160–8169.

Ye, M.D., Zheng, D.J., Lv, M.Q., Chen, C., Lin, C.J., Lin, Z.Q., 2013. Hierarchically structured nanotubes for highly efficient dye-sensitized solar cells. Adv. Mater. 25, 3039–3044.

Zhang, J., Sun, P., Jiang, P., Guo, Z., Liu, W., Lu, Q., Cao, W., 2019. The formation mechanism of tio_2 polymorphs under hydrothermal conditions based on the structural evolution of [ti(OH) h (H_2o) 6-h] 4-h monomers. J. Mater. Chem. C 7, 5764.

Zhao, Z.W., Guo, Z.P., Wexler, D., Ma, Z.F., Wu, X., Liu, H.K., 2007. Titania nanotube supported tin anodes for lithium intercalation. Electrochem. Commun. 9, 697–702.